# IET Smart Grid

## Special issue
## Call for Papers

**Be Seen. Be Cited.
Submit your work to a new
IET special issue**

Connect with researchers and experts in your field and share knowledge.

Be part of the latest research trends, faster.

**Read more**
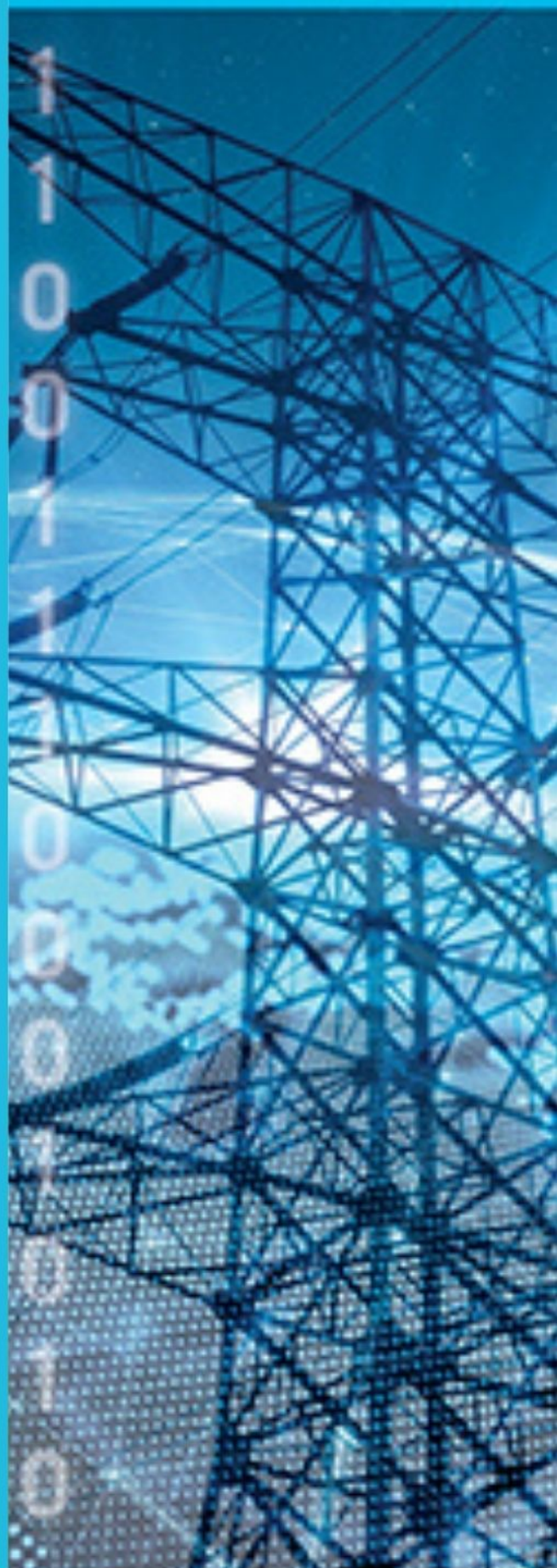
**IET** The Institution of Engineering and Technology

**ORIGINAL RESEARCH**

# Real-time resilient microgrid power management based on multi-agent systems with price forecast

**Marcos Eduardo Cruz Victorio** ⓘ | **Behzad Kazemtabrizi** | **Mahmoud Shahbazi** ⓘ

Department of Engineering, Durham University, Durham, UK

**Correspondence**

Behzad Kazemtabrizi, Department of Engineering, Durham University, Stockton Rd, Durham DH1 3LE, UK.
Email: behzad.kazemtabrizi@durham.ac.uk

**Abstract**

Microgrids have emerged to diversify conventional electric generation using small-scale distributed generation. Large efforts have been put into designing control strategies to optimise the power schedules of microgrids, however, verification that such control systems also are reliable in terms of stability during normal operation and fault conditions is needed. This study presents a hierarchical distributed control system that fulfils these conditions for an AC microgrid. The stability maintained by proposed controller, considering the large signal model, is analysed with the use of Lyapunov's direct method. Resilient control distribution is achieved by the implementation of suitable forecast models and fault-tolerance mechanisms to avoid single points of failure. The resilience of the control system is verified with the use of graph theory. The stable and resilient operation of the proposed control system is tested by a real-time microgrid model implemented with an OPAL-RT real-time simulator, combined with a communication network built with Raspberry Pis, testing the control system presented under normal and faulty conditions. Simulation results show a stable operation in terms of voltage and frequency in both conditions, resilient operation is shown for the faulty condition case. Additionally, cost minimisation performance is included to validate optimal power management capabilities.

**KEYWORDS**

AC microgrid, artificial neural network, auto-regression, Lyapunov stability, Markov chain Monte Carlo, multi-agent system, price forecast

## 1 | INTRODUCTION

As the global population levels grow, the electricity demand and thereby carbon emissions are ever increasing. As a consequence, more countries are adopting policies to combat negative effects of rising carbon emissions. To this end, several types of renewable energy resources are being integrated into the electric system. The microgrid has emerged as a viable option to integrate new small-scale electricity generation capacity, most of which are based on renewable energy resources, into the grid as distributed generation. In this context, a microgrid is a system capable of generating or storing its own energy and supplying its own electric demand autonomously, in which local sources of electricity are known as Distributed Energy Resources or DERs.

Naturally, there is a need for controlling the interactions (i.e. power/energy transactions) of the DERs within the microgrid and with various stakeholders including the consumers, and/or the distribution network operator to which the microgrid is connected. Moreover, most DERs, especially those based on renewable resources may be equipped with Energy Storage Systems (ESS) which requires coordination and control of interactions between the DER and their corresponding energy storage systems as well.

In most circumstances, the control system of the microgrid is organised in a hierarchical structure comprising of different control layers [1–3]. Each preceding layer provides the required set-points (references) for its immediate layer succeeding it.

Typically, three layers are used for microgrid control [1–3]. The primary control layer represents the relevant DER

controllers, which regulate the voltage and frequency of each individual source. The secondary control layer sends the power references to the primary layer given some objective for the microgrid, such as power sharing or cost optimisation. Finally, the tertiary layer coordinates the operation of multiple microgrids or the operation of the microgrid within the distribution system. This paper presents the design and performance of the first two control layers namely, the primary and the secondary layers.

As the primary control layer is designed for the regulation of the DERs, the stability of the entire system depends on the appropriate design of the primary controllers.

For the case of AC microgrid control systems, the stability of operation is verified only by simulation. There are few examples of the mathematical analysis of the AC Microgrid, and most of these analyse droop-based systems [4, 5]. The stability of the AC microgrid, considering the non-linear elements in the circuit, can be verified using the large signal model. This is necessary to capture the non-linear behaviour of the electrical power as a function of the voltage and phase angle during the transient states [6]. This analysis can be implemented with the help of the Lyapunov's methods [4, 5].

The use of the Lyapunov method to guarantee the stability of a microgrid controller can be found in control systems such as in refs. [7, 8]. Similarly, in ref. [9] the Lyapunov stability method is applied to a single DER as a general analytical tool for microgrids of any arbitrary number of buses. In ref. [10] the Lyapunov method is used to improve the current response of a DER under normal and faulty conditions in the microgrid's circuit, considering the current response of the AC microgrid. However, in this studies the reliability of the control system was not considered.

Once stable operation is guaranteed, the secondary control layer can be designed to direct the primary controller to satisfy the objective of the secondary control layer. Depending on the type of control used in the microgrid, among other objectives, the power schedule generated could be used to regulate the power sharing of the DERs, or as in this paper, the power schedule generated is used to maximise the economic benefit of the DER owners within the microgrid.

The secondary control layer can be designed to mimic the centralised control schemes of a utility transmission grid, in which a single control unit regulates the operation of the interactions between stakeholders within the system [11]. However, this approach has two overarching flaws (i) it leaves the entire microgrid's operation vulnerable to a single point of failure and (ii) it creates a privacy vulnerability as all the information of the system must be shared to generate an optimum power schedule.

Both of these disadvantages are avoided with a distributed control design of the secondary control layer. In contrast to a centralised control structure, in a distributed control structure, each distributed controller, which regulates a DER in the microgrid, has more autonomy to solve local power scheduling problems while is also capable of cooperating with the rest of the microgrid, forming a communication network that, as a whole, reaches a global objective. The ability of the distributed control to respond in real-time is still needed to be demonstrated as examples of these designs are not yet fully validated for real-time scenarios [12].

Multi-Agent System (MAS) control has been implemented to realise distributed control for microgrids, where an agent is a single unit of artificial intelligence capable of interacting with other agents. The actions an agent can take are programmed in what is known as behaviours. The agents are organised in containers, and the collection of all containers of the same MAS is referred to as the MAS platform. It follows that in the context of a distributed hierarchical control system, a MAS platform applies to the secondary control layer. Examples of this approach are found in refs. [2, 13–15] where the MAS was used for a consensus protocol for power flow distribution between a central controller and distributed primary controllers.

It is obvious that there needs to be a communication network implemented to enable efficient communication between agents. However, the existence of such a network may introduce a single point of failure in the absence of any resilience or fault-tolerance mechanism in the secondary control layer. To solve this, it is necessary to include a fault-tolerance mechanism in the secondary control layer, which allows the control system to continue operation even in the event of a failure in the communication network.

In the case of MAS platform, it is possible to implement a restoration service with these properties, adding resilience to the secondary control layer [2]. These services can be analysed with the use of graph theory, in particular, with the use of the characteristic polynomial (or the L-polynomial) of the underlying connection matrix, also known as the Laplacian, of the graph representing the communication network between agents [16, 17].

The restoration service in this paper is based on periodic communication between the distributed controllers. While some authors consider this type of communication more computationally expensive [18], this type of communication allows the detection of broken communication links or unresponsive controllers, allowing the rest of the system to remove such components from the communication network and continue operation.

To increase the reliability of distributed generation in the form of microgrids, it is important to verify the stability of such systems during transient and steady state. The stability of the system results from the interaction of the primary control layer with the physical layer, in the case of hierarchical control schemes. Validation of the primary control layer is often limited to simulation of the proposed controllers, however this approach is limited as can only show stability for the conditions set in the specific case study. Additionally, the stability analysis is often limited to linear systems that may neglect the non-linear nature of microgrid's power flow.

The Lyapunov stability analysis, on the other hand, can be used to mathematically define the conditions for stability of a non-linear system. For the case of non-linear systems, there are two methods based on Lyapunov analysis. The first one is based in the linearisation around the equilibrium point,

however this method is valid for stability in the small-signal case. The second method is based on verification of Lyapunov's theorems of the equilibrium point in combination with Lyapunov functions. Given that the second method captures the non-linear properties of the system, the second method is useful to analyse the stability of the system for the large-signal case as well. The equations used for the Lyapunov's second method will be presented in Section 3.

Once the microgrid's control system integrates stability and resilience as part of its design, it is critical that the operation of the microgrid is economically optimal to further facilitate the transition from centralised to distributed generation as a viable way to combat negative effects of increased carbon emissions and aid with decarbonisation of the energy systems.

To achieve cost-effective power management in the microgrid, the secondary control layer realised by the MAS platform generates the power schedule to minimise cost of supply in the medium term.

However, given some components in the system such as batteries cannot change their states of charge instantaneously and given that there is an inherent uncertainty from variability of electricity prices from the main grid, it is necessary to implement an efficient and yet fast forecast process in the secondary control layer, considering the conditions imposed by the distributed design.

Total supply Cost minimisation of the microgrid in a distributed environment requires that the power management does not rely on a centralised signal, therefore, auto-regression forecast models are proposed in this paper as a suitable solution, as they can perform the forecast using only local information [19]. The use of auto-regressive models for forecast requirements in a MAS platform has been reported in Ref. [20], where wind speed and wind power generation forecast were realised by an Auto regressive External (ARX) model for one-minute ahead predictions. In ref. [21] an ARX model is used as part of a day-ahead electricity price forecast; however, the external input requirement increases the centralisation of the forecast, making these type of methods unsuitable for distributed control.

Markov Chain Monte Carlo (MCMC) methods are Bayesian methods used to estimate the parameters of a Probability Density Function, given some historical data [22]. Applications of MCMC methods for distributed generation to estimate solar generation can be found in ref. [23], and in ref. [24] for wind speed forecasting.

The Non-linear auto-regression Network (NARNET) is used to generate future time steps in a non-linear time-series, without the need of any other external input [25]. With regards to the way of organising the layers of the NARNET, there are three main ways, having a single layer, layers connected in series and layers connected in parallel [26, 27].

Additionally, applications of Monte Carlo methods and Artificial Neural Networks (ANNs) have appeared in the literature, such as in ref. [28], where a centralised energy management system used a deep neural network as a simulation tool to extract samples of a multi microgrid system's response to price signal. By doing many iterations and treating the data with a Monte Carlo method, the system was capable to minimise peak to average ratio and maximise energy profits for the Distribution System Operator. The MCMC and NARNET methods are therefore studied in this paper to achieve cost minimisation in the microgrids' distributed control.

Although microgrid control systems in the literature are validated for one or two of the elements shown in Figure 1, there is still a need to verify that microgrid control systems contain all of the elements to achieve resilient and cost-effective operation of distributed generation. This paper aims to demonstrate that the proposed control system has all of these properties, with the use of mathematical analysis and real-time simulation models.

## 1.1 | Key contribution

The key contribution of this work can be summarised as follows:

- Proposition of a novel AC microgrid hierarchical control system that is simultaneously stable, resilient to communication failure and suitable for real-time distributed control with supply cost minimisation capabilities under price uncertainty. The stability of the AC microgrid, with a distributed control system is verified with the use of Lyapunov's method at the primary control layer in combination with the physical layer. The secondary control layer implements a MAS and auto-regression forecast models for optimal power management, with resilient operation capabilities under normal and faulty conditions, analysed with the use of graph theory.
- Analysis of the ability of the proposed control system to achieve supply cost minimisation with the use of electricity price forecast suitable for real-time distributed control. Improvement of price forecast models for distributed real-time microgrid control for the UK's electricity is also presented. The forecast models are compared in terms of total supply cost achieved when integrated in the control system.
- Validation of the stability, resilience and cost minimisation capabilities of the proposed control system with the use mathematical models and real-time simulation models, including scenarios under normal and faulty conditions at the communication network of the microgrid's control system. The simulation model of the physical layer and the primary control layer is realised by an OPAL-RT real-time simulator while the communication network at the secondary control layer is realised externally by a network of Raspberry Pi's.
- Finally, the performance of the entire control system operation is verified in real-time operation, with the use of an OPAL-RT simulator for the microgrid model and the primary control layer, and a network of Raspberry Pi's for the secondary control layer.

The rest of the paper is organised as follows: Section 2 describes the hierarchical control framework and all the
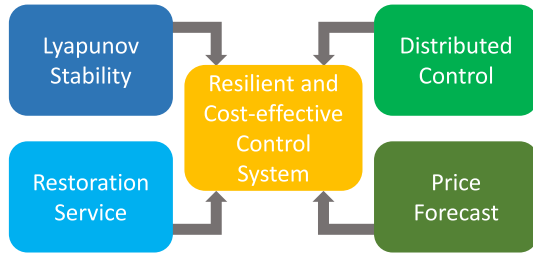
**FIGURE 1** Elements of the distributed control System model implementation in real-time simulation.

mechanisms required to achieve cost minimisation. Section 3 elaborates on the primary control stability and on the resilient design of the secondary control. Section 4 defines the test case for the microgrid control application. Section 5 shows the simulation and results details and the paper finalises with the conclusion in section 6.

## 2 | HIERARCHICAL CONTROL

As mentioned before, hierarchical control for microgrids is divided in two layers, in this paper, the secondary control layer is used for the power management of the microgrids, by sending the power references to the primary control layer, which in turn regulates the electrical operation of the DERs in the microgrid in real-time.

The next subsections present the application of each layer in terms of the cost minimisation objective for real-time distributed control. The stability analysis of the primary control layer and resiliency of the secondary control layer is then explained in more detail in the latter sections of the paper.

### 2.1 | Primary control

The primary control in this paper has the objective of regulating the voltage and phase angle of each DER whilst maintaining the frequency constant, as opposed to decentralised droop-based methods, in which the active power flow of each DER is proportional to the frequency, mimicking the inertia of rotational machines. The primary control layer in this paper operates by following the power references (set-points) generated from the secondary control layer as shown in the blue regions in Figure 2, which are scheduled in such a way to achieve an optimal cost operation.

Each primary controller in this work regulates the voltage and frequency response of each DER and ESS to be maintained within the UK standard, of $400 -6\% + 10\% \ V_{line}$ and $50 \pm 1\%$ Hz. The primary controller consist of two control loops, the first one regulates voltage and the second one regulates power. This design allows stable interaction between the electrical circuit of the DERs, which extends to the microgrid, and the secondary control layer. The stability of this design will be presented in later in this paper.

The design of this control layer is required to be compatible with the distributed control of the secondary control layer. For this reason, the primary controllers are designed to operate using the dq0 reference frame. This allows the primary controllers to calculate the power flow of the system locally, and in turn regulate the bus voltage and phase angle of their DERs according to the references sent by the distributed secondary controller.

Even though the controller can function with only voltage references, a power schedule can be supplied as power references to achieve secondary level objectives, in this mode of operation, the primary control layer adjust the voltage and phase angle of each DER and ESS to follow their power schedule. This process is presented in the following subsection.

### 2.2 | Secondary control

The objective of the secondary control layer in this paper is the minimisation of the total supply cost to the microgrid by solving the global cost minimisation problem and generating the corresponding power references of the DERs for the primary control layer. The design of the secondary control layer, as mentioned previously, must be compatible with distributed control and resilient operation requirements, for which the price forecast methods required for optimal operation are solved locally using only available historical data.

To achieve distribution of the secondary control layer, the global cost minimisation problem is broken down into local problems such that each task can be assigned to the individual agents in the MAS platform that realise the secondary control. Once the power schedule is obtained by solving the cost minimisation problems of each DER and ESS, the corresponding agent sends the power references to each of the primary controllers of the DERs. The secondary control layer is depicted as the grey region in Figure 2. The agents used for the secondary control layer and their organisation is explained in the next subsection.

#### 2.2.1 | Global cost optimisation

The operation of the secondary layer as a whole has the objective of minimising the total supply cost of the microgrid, considering buying and selling from/to the grid, from the point of view of the owners of the DERs and ESS.

To minimise the cost of supply of the entire microgrid the following optimisation problem is solved:

$$\min \quad \sum_i \sum_j c_j\big((P_j(i)\big), \qquad \forall j \in \mathcal{K} \wedge \forall i \in \mathcal{N} \qquad (1a)$$

$$\text{s.t.} \quad P_{jmin} \leq P_j \leq P_{jmax}, \qquad (1b)$$

$$SOC_{min} \leq SOC \leq SOC_{max}, \qquad (1c)$$
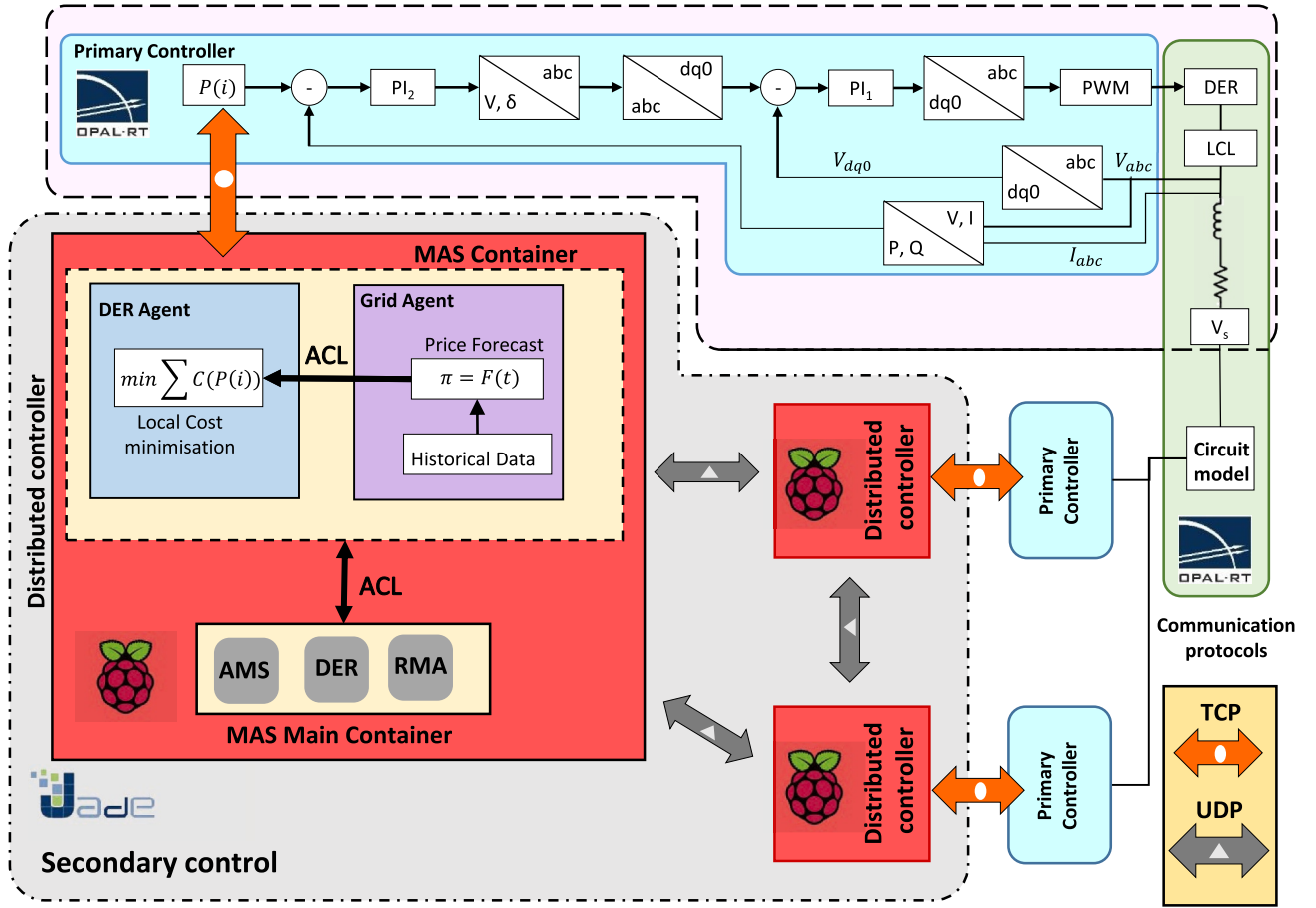
**FIGURE 2**  Distributed hierarchical control system architecture as presented in this paper and implementation in a real-time simulation environment. The pink region illustrates the primary control layer whose stability is verified using the Lyapunov's direct method. The grey region shows the secondary control layer containing the MAS platform together with its underlying communication structure. The reliability of the MAS platform communication structure is analysed with the help of graph theory. The green region represents the physical microgrid model which is implemented in an OPAL-RT simulation environment. The MAS platform is implemented using a network of Raspberry Pis.

$$SOC(i+1) = SOC(i) - \eta P(i), \qquad (1d)$$

$$P_L(i) - \sum_j P_j(i) = 0, \qquad \forall j \in \mathcal{K}, \forall i \in \mathcal{N}, \quad (1e)$$

$$[P\,Q] \in [P(X)\,Q(X)], \qquad \forall X \in D_{\mathcal{X}} \qquad (1f)$$

where $c_j(.)$ is the cost function of each source $j$ of DERs and ESS, $\mathcal{K}$ is the set containing all the generation sources. $P_j$ and $Q_j$ are the active and reactive powers sent by source $j$ at each hour $i$ for a period $N$, in the set $\mathcal{N} = \{1\ldots N\}$. Each power $P_j$ is bounded by a minimum $P_{jmin}$ and maximum $P_{jmax}$. Similarly, the State of Charge (SOC) is bounded by a minimum $SOC_{min}$ and a maximum $SOC_{max}$, the SOC depends on its previous value, the power $P(i)$ and $\eta$, which models the capacity and round trip efficiency of the ESS. The Load $P_L$ and generation in the microgrid must be equal. The last constraint is used to guarantee Lyapunov stability and limits the power references sent to the primary control, expressed in terms of the state variable $X$ in the domain $D_{\mathcal{X}}$, which will be explained in detail in the next section.

The cost minimisation mechanisms must be designed to work in a distributed control setting, considering the fact that the system needs to do price forecast to generate the power references for the DERs and ESS. These requirements are addressed by the MAS design and price forecast models presented in the next subsections.

## 2.2.2 | Multi-Agent System

The MAS approach is used to realise the distributed secondary control. In every MAS application, there are three general agents for the operation of a distributed control, namely the Agent Manager Systems (AMS), the Directory Facilitator (DF), and the Remote Monitoring Agent (RMA). The AMS is in charge of creating and terminating agents, the DF serves as the yellow pages, receiving requests and offers for services from the rest of agents, informing the relevant agents when there is a match for service and demand. In other words, it allows the formation of the communication networks among the rest of the agents. The container that hosts the AMS and DF agent is

the Main container. The RMA serves as a communication channel between containers in different computers, which contributes to control distribution at the communication network level.

The global cost optimisation is realised by the agents designed for the microgrid operation by solving the local optimal operation of each part of the microgrid. Subsequently, through cooperating with each other, the agents generate the power schedule to be sent to each of the primary controllers. The agents communicate with each other using Agent Communication Language (ACL) messages, sending and receiving information such that the entire MAS platform is capable of generating a power schedule that minimises total supply cost for the microgrid. Figure 2 illustrates the communication between the agents and the control layers as arrows.

In this paper, each DER and ESS in the microgrid have a corresponding agent container with the agents used for distributed microgrid control. The three agents designed specifically for the microgrid control presented in this paper are described as follows:

**DER agent**: This agent is used to calculate the power references of each DER based on the electricity price forecast and the DER's cost function. The DER agent behaviour is an internal loop of 10 milliseconds that manages the communication with the DF agent, AMS and corresponding Grid Agent (GA). Once all the messages are sent and received, the agent uses the price forecast $\pi(i)$ at hour $i$, provided by the GA, and the DER cost function $c_j(.)$ to generate the corresponding power references and then send them to the primary control using TCP/IP. The power schedule is the solution of the following local cost minimisation problem:

$$\min \quad \sum_i \pi(i)\big(P_{jmax} - P_j(i)\big) + \sum_i c_j\big((P_j(i)\big), \forall i \in \mathcal{N} \quad (2a)$$

$$\text{s.t.} \quad P_{jmin} \leq P_j \leq P_{jmax}, \quad (2b)$$

$$[P\ Q] \in [P(X)\ Q(X)], \ \forall X \in D_X \quad (2c)$$

The cost function of each DER is:

$$c_j\big(P_j(i)\big) = \begin{cases} c_B P_j(i) + c_C + c_s & P_j(i) \neq 0 \\ 0 & P_j(i) = 0 \end{cases} \quad (3)$$
$$\forall i \in \mathcal{N} \wedge \forall j \in \mathcal{K}$$

where the start-up cost function $c_s$ is:

$$c_s = \begin{cases} s & \big(P_j(i-1) = 0 \wedge P_j(i) > 0\big) \vee P_j(1) > 0, \\ 0 & otherwise \end{cases}, \quad (4)$$
$$\forall i \in \mathcal{N} \wedge \forall j \in \mathcal{K}$$

where $c_B$ and $c_C$ are generator specific cost parameters and $s$ is the start-up cost [29].

The local problem solved by the DER agent is limited to minimising the total supply cost of a specific source $j$ with respect to the price forecast, along a period $N$ in $\mathcal{N}$. The DER agent programmed behaviour considers if the start-up cost is worth to be paid based on the future prices and the current state of the DER, especially when the price forecast varies closely to $c_B P_{jmax} + c_C$.

**ESS agent**: This agent regulates the charge and discharge of the battery, based on the electricity price forecast, by sending the power reference signals to its primary controller according to the following local total cost minimisation problem:

$$\min \quad \sum_i \pi(i)\big(P_{jmax}(i) - P_j(i)\big), \forall i \in \mathcal{N} \quad (5a)$$

$$\text{s.t.} \quad P_{jmin} \leq P_j \leq P_{jmax}, \quad (5b)$$

$$SOC_{min} \leq SOC \leq SOC_{max}, \quad (5c)$$

$$SOC(i+1) = SOC(i) - \eta P(i), \quad (5d)$$

$$P_L - \sum_j P_j = 0, \forall j \in \mathcal{K} \quad (5e)$$

$$[P\ Q] \in [P(X)\ Q(X)], \ \forall X \in D_X \quad (5f)$$

To solve the local cost minimisation problem of the ESS, considering the dynamic behaviour of the SOC, the ESS agent determines the power references based on the current electricity price, the price forecast, the ESS model and the current SOC.

The power references are generated by modelling the battery in advance to steer the SOC such that a power schedule is available by applying offline Model Predictive Control. The ESS agent then applies energy arbitrage for supply cost minimisation. This allows, for example, steering the SOC to be at maximum at the moment of peak price or to be at minimum at the moment of lowest grid price, to maximise profits from selling energy and minimising costs from buying energy from the grid. To do this, the ESS agent requests a price forecast sufficiently long from the GA (explained in the next subsection), such that the ESS agent always has enough time to completely charge or discharge the battery to maintain optimal operation in terms of cost. The DER and ESS agents operate in separate MAS containers, solving their optimisation problems locally based on the price forecast supplied by their corresponding GA, illustrated in Figure 2.

**Grid Agent**: The GA at each agent container, which corresponds to each bus with distributed generation in the microgrids, generates a price forecast signal based on historical price data stored locally to be sent to the corresponding DER and ESS agents.

This agent is created in each agent container, as requested by other DER or ESS agent to the AMS, such that each container is independent of external control signals in terms of

microgrid control, in line with distributed control requirements. All of the agents for microgrid control subscribe to the DF agent, such that they can send and receive the corresponding ACL messages for microgrid's power management. The resiliency of the MAS platform in case of a faulty main container is presented in the next section.

Two price forecast models where studied in this work and applied to the GA, as presented in ref. [30], the NARNET and the Weighted Average (WA). Both forecast methods are presented in the next two subsections.

## 2.2.3 | Forecasting methodologies

The price forecast models presented in this section are suitable for distributed control, such that operation of each DER does not depend on an external signal, which could represent a single point of failure for the operation of the microgrid. The results shown our previous work [19] demonstrate that the difference in having independent forecasts in each DER bus is minimal in terms of cost. This in turn affirms the use of independent forecast signals generated locally for distributed control purposes, even with the small variations in the price forecast models used. The two forecast models used in this paper are explained in the following:

**Weighted Average:** The WA price forecast model is composed by previous prices, parameters obtained using the MCMC method, and weight coefficients. The coefficients are obtained by applying the Quasi-Newton numerical solver. The WA price forecast model $F_1$ is described as:

$$F_1 = w_1 p_{i-24} + w_2 p_{i-168} + w_3 \overline{\pi_a} + w_4 \overline{\pi_b} + w_5 \overline{\pi_c} \quad (6)$$

where $p_{i-24}$ is the price for the previous day, $p_{i-136}$ is the price for the previous week, $\overline{\pi_a}$ is the average price for the same day of the week, $\overline{\pi_b}$ the average price of the season and $\overline{\pi_c}$ is the average price of the entire data. The averages $\overline{\pi_x}$ are estimated from the UK data set using the MCMC with Metropolis–Hastings algorithm [30, 31], and the weights $w_j$ are obtained by solving a least squares regression problem:

$$\min_{\mathbf{W}} \sum_i \left( p_i - \pi_i(\mathbf{W}) \right)^2, \forall i \in \mathbf{m} \quad (7a)$$

where $\mathbf{W}$ is a vector containing the weights of Equation (6) for the hours $i$ in the period $m$ represented by the data set $\mathbf{m} = \{1 \ldots m\}$.

**NARNET:** The NARNET is trained using the Levenberg–Marquardt back-propagation algorithm, by randomly separating 15% of the time steps for training, 15% for validation and the rest for evaluation.

For this forecast method, the daily prices are treated as the input vector for the ANN, which in turn outputs the next day price prediction, using a delay size of 1 week and two layers as shown in Figure 3. This means that the ANN stores the information of the previous prices as part of the auto-regression
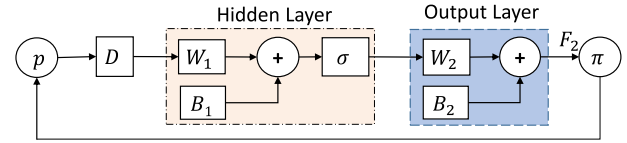


**FIGURE 3**   Non-linear auto-regression Network (NARNET) architecture applied by the GA.

model. The NARNET price forecast method $F_2$ is formulated as follows:

$$F_2 = W_2 \sigma(W_1 D + B_1) + B_2 \quad (8)$$

where $W_1$ and $W_2$ are the neuron weight matrices, $B_1$ and $B_2$ are the bias vectors of each layer of the NARNET, and $D$ is the delay vector, or 'memory' of the NARNET, defined as:

$$D(t) = \left[ p_{t-1} \ p_{t-2} \cdots p_{t-t_d} \right]^T \quad (9)$$

where $p_i$ are the prices at each hour $i$, storing up to $t_d$ hours and $\sigma$ is the logistic sigmoid activation function of the hidden layer [32]:

$$\sigma(W_1 D + B_1) = \frac{1}{\left(1 + e^{-W_1 D + B_1}\right)} \quad (10)$$

As the NARNET operates, the values in $D$ shift positions with the next time step, eliminating the oldest information first, while $D$ is updated through the network's feedback loop. The NARNET architecture is shown in Figure 3.

For the MAS application, the GA implements either Equation (6) or Equation (8) for the price forecast, as $\pi = F(t)$, which is then sent to the corresponding DER or ESS agent to generate the power references for the primary control.

## 3 | RESILIENCY AND STABILITY IN A DISTRIBUTED CONTROL ENVIRONMENT

Even though the microgrid must enable the optimal power scheduling for cost minimisation, it must also be able to maintain stable operation under load and DER variations. To this end, the limits of operation of the primary control are defined for asymptotic stability operation, using Lyapunov stability analysis, to guarantee that the primary control layer is stable.

To guarantee resilient operation of the secondary control layer in the event of loss of one of the nodes of the communication network of the secondary control, a restoration service is implemented, which is analysed in terms of graph theory, with the MAS communication network modelled as a connected graph. The mechanisms for resilient and stable microgrid operation of each layer are explained in the following subsections.

## 3.1 | Lyapunov stability

The following part will outline the necessary conditions to guarantee the steady state stability of the microgrid, analytically using Lyapunov's direct method, which is required for non-linear systems, as is the case here. The analysis is done considering a distributed control environment in an AC microgrid. The analysis is applied to the pink region shown in Figure 2.

The system stability can be analysed by analysing the stability of each control loop as follows:

### 3.1.1 | Inner loop

The inner loop regulates the voltage of the power converter with the aid of the LCL filter depicted in the green region of Figure 2. The dynamics of the inner loop consider the effect of the LCL filter and the line connecting the two buses. The stability is established by the stability of the current with respect to the voltage output from the power converter $V_U$ and the grid bus voltage $V_S$:

$$V_U = L_U \frac{dI_U}{dt} + V_C \tag{11}$$

$$V_C = \frac{1}{C} \int (I_U - I_S) dt \tag{12}$$

$$V_C = L_S \frac{dI_S}{dt} + RI_S + V_S \tag{13}$$

where $I_U$ is the converter output current, $I_S$ is the bus current, $L_U$ is the inductance at the converter side, $L_S$ is the inductance at the bus side, $C$ is the capacitance, and $V_C$ is the capacitor voltage of the LCL filter. Transfer functions for $I_S$ are:

$$T_1 = \frac{I_S}{V_U} = \frac{1}{L_U L_S C s^3 + R L_U C s^2 + (L_U + L_S)s + R} \tag{14}$$

$$T_2 = \frac{I_S}{V_S} = -\frac{L_U C s^2 + 1}{L_U L_S C s^3 + R L_U C s^2 + (L_U + L_S)s + R} \tag{15}$$

As there are no sign changes in the terms of the denominators, and all terms are positive, all roots have negative real parts, which in turn guarantee open loop stability with respect to $V_S$. In a similar manner, it is possible to find gains for PI control such that the system is closed loop stable with respect to $V_U$.

### 3.1.2 | Outer loop

As the inner function is stable, the outer loop must be asymptotically stable to establish stability of the entire cascade control [33]. The outer loop models the dynamics of power flow between buses according to the following equation:

$$S_S = 3 \frac{V_S}{R^2 + \omega^2 L^2} ((RV_S - RV_R cos\delta - \omega L V_R sin\delta)$$
$$+ i(RV_R sin\delta + \omega L V_S - \omega L V_R cos\delta)) \tag{16}$$

where $S_S$ is the apparent power sent, $V_S$ is the sending bus voltage, $V_R$ is the receiving bus voltage, $\delta$ is the phase angle between $V_R$ and $V_S$, $\omega$ is the angular velocity, $R$ is the resistance of the line, and $L$ is the inductance of the line.

Selecting $V_R$ and $\delta$ as the variables and treating the rest of parameters as constant, the following system of equations can be formulated for the active power $P$ and reactive power $Q$ sent from the converter to the bus:

$$P(V_R, \delta) = K_1(RV_R cos\delta + \omega L V_R sin\delta - RV_S) \tag{17}$$

$$Q(V_R, \delta) = K_1(\omega L V_R cos\delta - RV_R sin\delta - \omega L V_S) \tag{18}$$

$$K_1 = \frac{3V_S}{R^2 + \omega^2 L^2} \tag{19}$$

By selecting the appropriate state variables, $X_1$ and $X_2$, the closed loop integral control is formulated as follows:

$$V_R = X_1 + V_S \tag{20}$$

$$-\delta = X_2 \tag{21}$$

$$P(X_1, X_2) = K_1(X_1(Rcos X_2 + \omega L sin X_2) + V_S(Rcos X_2 + \omega L sin X_2) - RV_S) \tag{22}$$

$$Q(X_1, X_2) = K_1(X_1(\omega L cos X_2 - R sin X_2) + V_S(\omega L cos X_2 - R sin X_2) - \omega L V_S) \tag{23}$$

$$\dot{X}_1 = -K_1(X_1(Rcos X_2 + \omega L sin X_2) + V_S(Rcos X_2 + \omega L sin X_2) - RV_S) \tag{24}$$

$$\dot{X}_2 = -K_1(X_1(\omega L cos X_2 - R sin X_2) + V_S(\omega L cos X_2 - R sin X_2) - \omega L V_S) \tag{25}$$

which has a solution in $\dot{X}(0) = 0$, where $X = [X_1 X_2]^T$. To demonstrate Lyapunov local Asymptotic Stability by the direct method, a candidate function $V$ must have the following properties [34, 35]:

$$V(0) = 0 \tag{26a}$$

$$V(X) > 0, X \neq 0, X \in D_X \tag{26b}$$

$$V(X) \to \infty, \|X\| \to \infty \tag{26c}$$

$$\dot{V}(0) = 0 \tag{26d}$$

$$\dot{V}(X) < 0, X \neq 0, X \in D_X \tag{26e}$$

The function $V$ and domain $D_X$ are selected as follows:

$$V(X) = 1/2X_1^2 + 1/2X_2^2, X \in D_X \quad (27)$$

$$D_X = \{X \in \mathbb{R} | V(X) \leq \alpha, \, 0 \in D_X, \, D_X \text{ is continuous}\} \quad (28)$$

As $V$ has infinitely many solutions, $D_X$ is constrained such that it delimits a closed contour inside one of the closed level curves at value $\alpha$ around the origin. To meet the properties of a Lyapunov function, the domain $D_X$ is defined to contain only one solution for $V(X) = 0$ and $\dot{V}(x) = 0$ at $X = 0$.

Calculating the derivative and substituting the time derivatives from the system in Equation (20) the following is obtained:

$$\begin{aligned}
\dot{V}(X) &= X_1\dot{X}_1 + X_2\dot{X}_2, X \in D_X \\
&= -K_1X_1(X_1(RcosX_2 - \omega LsinX_2) \\
&\quad + V_S(RcosX_2 - \omega LsinX_2) - RV_S) \\
&\quad - K_1X_2(X_1(\omega LcosX_2 + RsinX_2) \\
&\quad + V_S(\omega LcosX_2 + RsinX_2) - \omega LV_S)
\end{aligned} \quad (29)$$

Given that Equations (27) and (29) meet the conditions set in Equation (26) $V$ is proven to be a Lyapunov function and therefore, the primary control is stable. The stability limits of the voltage imply a stability limit in the power that can be exchanged from one bus to another in the grid, as the voltage drop is directly proportional to the current in the cable and in turn, proportional to the power flow.

Figure 4 shows a rendering of $\dot{V}(X)$ with the level curves on top, showing that the derivative is concave with a single root at 0 for a domain that delimits any of the closed level curves.

Figure 5 shows the level curves of $\dot{V}$ overlaid with the trajectories of $\dot{X}$ to show that the system is locally asymptotically stable if the starting point is inside one of the closed level curves for an arbitrarily small error as all trajectories, shown as the blue arrows, point towards $X = 0$.

To guarantee that the two loops of the primary controller do not interfere with each other, the time domain response of the line current $I(t)$ between the buses is calculated:

$$\sqrt{2}V_Ssin(\omega t) = RI(t) + L\frac{dI(t)}{dt} + \sqrt{2}V_Rsin(\omega t + \delta) \quad (30)$$

With Laplace transform equation:

$$I(s) = \frac{K_2s}{s^2 + \omega^2} + \frac{K_3}{s^2 + \omega^2} + \frac{K_4}{\frac{R}{L} + s} \quad (31)$$

where $K_2$, $K_3$, and $K_4$ are constants that are obtained by solving the following matrix:
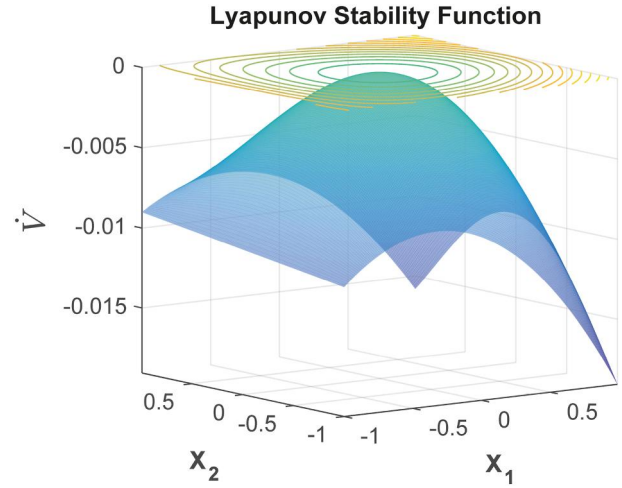


**FIGURE 4** Visualisation of the derivative of the Lyapunov function. This figure illustrates the negative semidefinite property of the derivative with respect of time of the Lyapunov function.
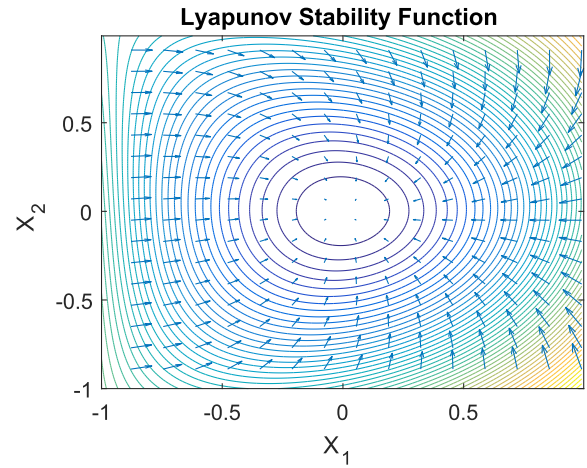


**FIGURE 5** Time trajectories of the state space of the outer loop according of the Lyapunov function. The vector field of the state space illustrates the attraction of the equilibrium point in the centre, demonstrating asymptotic stability.

$$\begin{bmatrix} L & 0 & 1 \\ R & L & 0 \\ 0 & R & \omega^2 \end{bmatrix} \begin{bmatrix} K_2 \\ K_3 \\ K_4 \end{bmatrix} = \begin{bmatrix} 0 \\ -\sqrt{2}\,V_Rsin(\delta) \\ \sqrt{2}\,V_S\omega - \sqrt{2}\,V_Rcos(\delta) \end{bmatrix} \quad (32)$$

With rest initial conditions, the current in time domain is expressed as follows:

$$\begin{aligned}
I(t) = \frac{\sqrt{2}}{L^2\omega^2 + R^2} &\Big( (L\omega(V_Rcos\delta - V_S) - RV_Rsin\delta)cos(\omega t) \\
&+ (R(V_S - V_Rcos\delta) - V_Rsin\delta L^{-1}\omega)sin(\omega t) \\
&+ (L\omega(V_S - V_Rcos\delta) + RV_Rsin\delta)e^{-\frac{R}{L}t} \Big)
\end{aligned}$$

$$(33)$$

It can be observed in Equation (33) that the transient state depends only on the last term, lasting $5R/L$ seconds, after which the current stabilises. If the current and voltage are stable, then the power will also be stable. This sets an upper limit on how fast the outer loop can operate and a lower limit on how slow the inner loop must be to prevent interference between each other.

As long as all the conditions described are met, the primary controllers will reach stable operation, however the system must also be resilient at the secondary control level. The next section will briefly review the mathematical theory used to assure the connectivity in the communication network of the secondary control and therefore guarantee its resilience.

## 3.2 | Secondary control resilience

In this section, the resiliency of the MAS communication network in the secondary control layer against faults is presented by modelling the underlying MAS communication network as a connected graph. The reliability analysis of the control system is applied to the grey region in Figure 2.

### 3.2.1 | Graph theory overview

A graph $G$ can be defined as the set of vertices $V_G$ and edges $E_G$ between them. They are represented by the equation:

$$G = (V_G, E_G) \tag{34}$$

For the set of vertices $V_G$:

$$V_G = \{v_1, \ldots v_n\} \tag{35}$$

Elements of $E_G$ are denoted as the pair of vertices $v_j$ and $v_i$ that are connected:

$$(v_i, v_j) \in E_G \tag{36}$$

For every graph $G$ we can define the adjacency matrix $A_G$ of size $|V_G| \times |V_G|$ with elements $a_{ij}$:

$$a_{ij} = \begin{cases} 1 & (v_i, v_j) \in E \\ 0 & (v_i, v_j) \notin E \end{cases}, \tag{37}$$

And the degree matrix $D_G$ of size $|V_G| \times |V_G|$ with elements $d_{ij}$:

$$d_{ij} = \begin{cases} N_i & i = j \\ 0 & i \neq j \end{cases}, \tag{38}$$

where $N_i$ is the amount of neighbours connected to node $v_i$. If the number of incoming edges is the same as the number of outgoing edges to every node, the graph is said to be balanced, which can be observed by verifying that the columns and rows

of the Laplacian matrix $L_G$ are equal to zero. Where $L_G$ is defined as:

$$L_G = D_G - A_G \tag{39}$$

The eigenvalues of the Laplacian, which have information about the graph, can be found by finding the roots of its L-polynomial according to the following:

$$|L_G - \lambda I| = 0 \tag{40}$$

where roots in terms of $\lambda$ are the eigenvalues. For the case of the L-polynomial $C_G$ of the union of disjoint subgraphs with individual L-polynomials $C_{G_i}$ up to **k** subgraphs, the equation is:

$$C_G = \prod C_{G_i} \, \forall \, \mathbf{i} \in \mathbf{k} \tag{41}$$

In a bidirectional communication network, such as in this case, the Laplacian matrix of the network's graph is singular, which leads to the existence of at least one eigenvalue $\lambda = 0$. It follows that the multiplicity of the eigenvalue $\lambda = 0$ indicates the number of separate subgraphs in the graph [36]. In other words, the smallest exponent of the L-polynomial reflects the number of networks in the system. If this exponent is 1, then the communication network is fully connected. The next subsection describes the mechanism implemented in the MAS to guarantee this mathematical property in the microgrid control under normal and faulty conditions.

### 3.2.2 | Restoration service

The proposed MAS control platform for the secondary control layer has this service installed to maintain the operation of the microgrid even during faulty conditions in one part of the system, which increases the reliability of the system overall, as the rest of the system remains in operation.

The fault-tolerance mechanism is triggered in any of the following cases, which are represented in Figure 6a. The communication link between containers is broken. b. Loss of agent container in the MAS c. Loss of the main container in the MAS.

For the first case, each side of the communication link will assume that the other side is no longer in the system. The side without a main container will launch a copy of the main container from the backup and assume leadership of the remaining container or containers in the network. This case results in two independent MAS applications working in the same microgrid.

In the second case, the primary controller keeps the last instruction sent by the secondary control at the corresponding lost container. The TCP/IP port would become available to be controlled by another container if there is a communication link available between the MAS and the primary control. If this is not the case, then the primary controller will follow the last instruction until the fault is cleared.
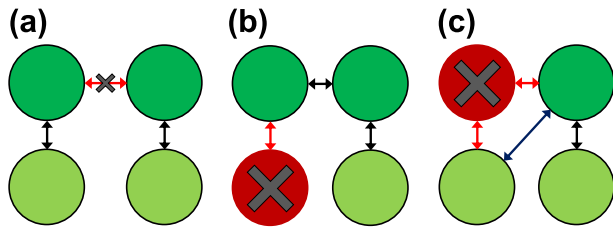
**FIGURE 6** Graph representation of modes of failure of the MAS communication network covered by the restoration service. The functioning nodes are represented by the green nodes and in red the faulty nodes and communication links. (a) The communication link between containers is broken. (b) Loss of an agent container in the MAS platform (c) Loss of the main container in the MAS platform

In the third case, the next backup in the User Datagram Protocol (UDP) ring launches a copy of the main container and assumes the address of the original main container. In this scenario, only the main container backups in the UDP ring will be notified, while the transition is seamless for the rest of the control system. There is also no effect from the primary controller point view as this type of fault can only be detected from the UDP ring.

This mechanism allows for fault-tolerance without a central controller, which is a common argument against distributed and decentralised controllers in terms of reliability. The hierarchical control with all the mechanisms described for optimal power schedule and resilient operation will be implemented in the test case for its evaluation.

## 4 | TEST CASE

The microgrid model used in this paper is composed of three controllable sources, a fuel cell, a Micro Turbine and a battery (ESS) as shown in Figure 7 with the same cost function parameters as presented in ref. [19]. The percentages show the load distribution and the numbers represent the buses that are being measured in the next section. The lines and load over time are the same as describe in ref. [19].

The microgrid model and the corresponding primary controllers are simulated in an OPAL-RT real-time simulator (Series OP5700[1] with an Intel Xeon E5, 4 cores, 3.0 GHz CPU. The software used to generate the simulation model is RT-LAB version 11.3.3.62. The secondary control is realised by the MAS platform, composed of two Raspberry Pi models 3B+ micro-computers, with a 1.4 GHz 64-bit quad-core ARM Cortex-A53 CPU and 1 GB of RAM, and a PC connected via Ethernet. For the price prediction, each computer is loaded with the UK price data from Nord pool from 29/12/2017 to 27/02/2020.[2] with resolution of one hour. Hardware used for training the forecast methods includes a desktop with an i7-6700 CPU at 3.40 GHz with 16 GB of RAM and a desktop
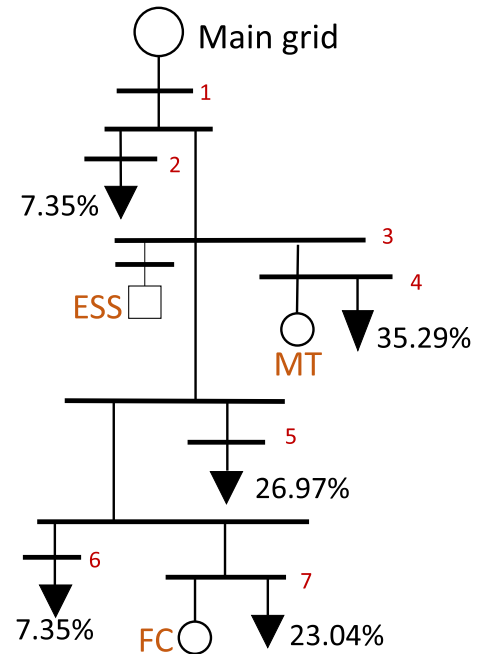


**FIGURE 7** Microgrid circuit test model.

with an i5-7500 CPU at 3.40 GHz with 8 GB of RAM. The software used for training is MATLAB R2019a (9.6.0.1099321) 64-bit. The NARNET is set to have 5 neurons in the hidden layer and a memory of 1 week. The real-time simulation is used to verify the viability of the control system in a much more realistic scenario than the offline simulation.

Two 24 h scenarios are run, in the first one, all the DERs operating and in the second one, a fault is induced at the ESS secondary control at 12 h to test the fault-tolerance mechanism of the system.

The total supply cost of the microgrid is calculated for each price forecast model and the real price, considered the ideal case, for each of the following cases: no weekends and no outliers, no weekends, no outliers and all data. Following the cost analysis done in our previous work [30], all the prices are adjusted to double and triple the values of the original data set, as the original data set is intended for wholesale market, which doesn't completely reflect the electricity price to the consumers. The price adjustment helps to visualise the effect of the accuracy of the forecast model in terms of cost with respect to available generation for sale. It is assumed that the microgrid can trade with the grid at the UK price to buy and sell energy, and in all cases the reactive power reference is set to zero.

## 5 | SIMULATION AND RESULTS

After the real-time simulation is completed the simulations results are organised in the simulation for the system under normal conditions and the system under fault conditions. Finally, the cost analysis is presented to validate the capability of the control system to achieve minimal costs based on the scenarios tested.

---

[1]For more information about this simulator please visit: https://www.opal-rt.com/resource-center/document/?resource=L00161_0337)

[2]For more information about market data offered by Nord Pool please visit https://www.nordpoolgroup.com

## 5.1 | System performance under normal conditions

It can be observed in Figure 8 that the primary controller adjust the voltage according to the changes of the load and accommodates for the power references from the secondary control simultaneously.

As is can be seen in Figure 9 the voltages for the buses across the microgrid remain within the current UK standard of voltage deviation tolerance of −6% and +10% for the distribution circuit.

Each of the primary controllers adjust the bidirectional active power flow and maintains the reactive power and frequency constant by adjusting the phase angle as shown in Figure 10.

For the secondary control layer, the calculation of the L-polynomial applying Equation (40), yields:

$$\lambda^6 - 12\lambda^5 + 51\lambda^4 - 92\lambda^3 + 69\lambda^2 - 18\lambda = 0 \qquad (42)$$

Which has only one eigenvalue equal to zero, and therefore the communication network is fully connected.

## 5.2 | System performance under fault conditions

For the fault case, the voltage variations are smaller as there is no power transfer from the ESS to the microgrid after the fault of the secondary control at noon. However, the voltage is stable for the rest of the day as seen in Figure 11.

Moreover, in Figure 12 it can be seen that the bus 3 voltage decreases as a result of the ESS not being used, and that the rest of the buses are adjusted for the remaining power flows. A similar adjustment can be seen for the phase angle in Figure 13. The microgrid remains stable and within the UK standard range in both cases in the transient state and steady state for the entire simulation.

With the loss of the ESS container, the L-polynomial of the communication network of the secondary control becomes:

$$-\lambda^5 + 10\lambda^4 - 33\lambda^3 + 40\lambda^2 - 23\lambda = 0 \qquad (43)$$

Which, as in the previous case only has one eigenvalue equal to zero and therefore indicates that the rest of the network remains fully connected.

## 5.3 | Cost analysis

This subsection evaluates the cost optimisation method developed to verify that the microgrid operates reliably and cost efficiently.

From the scenarios discussed in the test case section, the total supply cost is obtained. Each of the scenarios is run with the WA method and the NARNET method implemented in
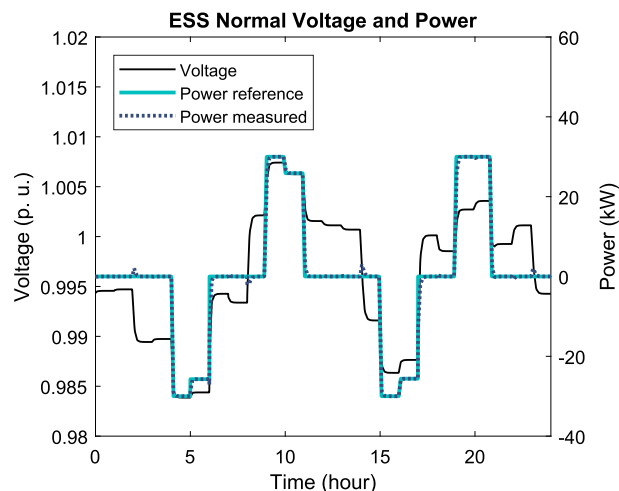


**FIGURE 8** Energy Storage Systems (ESS) control response under normal operation.
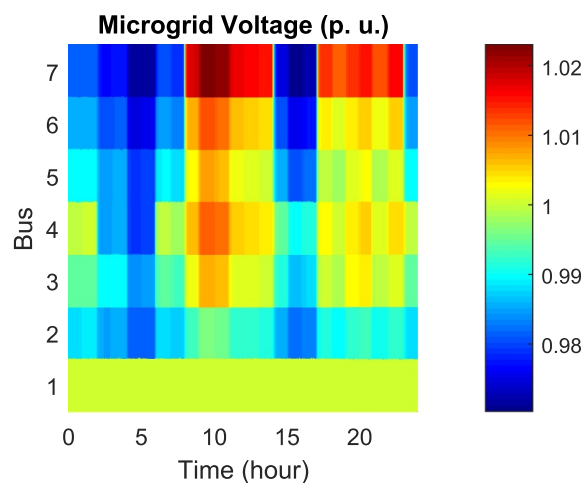


**FIGURE 9** Microgrid Voltage response under normal conditions. Colour illustrates voltage p. u. at each bus over time.
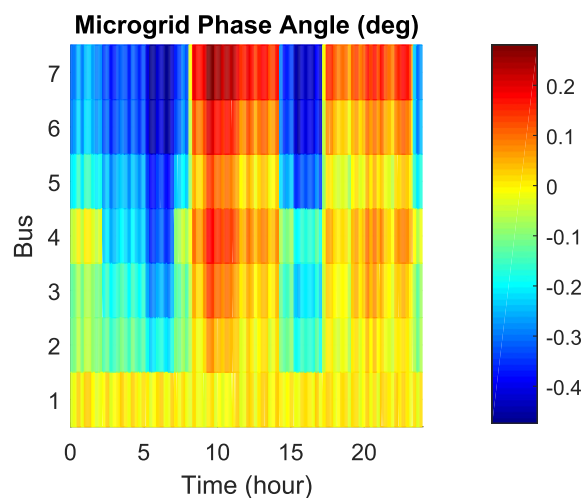


**FIGURE 10** Phase angle response across the microgrid under normal conditions. Colour indicates phase angle at each bus over time.
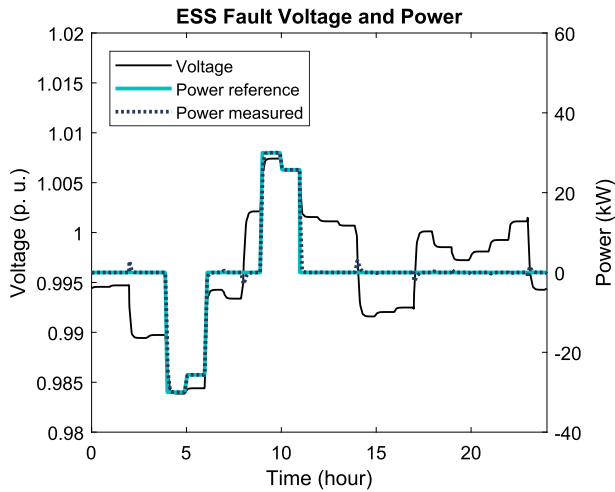
**FIGURE 11** Secondary Energy Storage Systems (ESS) control response with fault at noon.



**FIGURE 12** Microgrid Voltage response under faulty conditions. Colour illustrates voltage p. u. at each bus over time.



**FIGURE 13** Phase angle response across the microgrid under Energy Storage Systems (ESS) faulty conditions. Colour indicates phase angle at each bus over time.

the GA and compared with the ideal case, where the forecast has no errors, in other words, the real price is known in advance. From the Quasi-Newton optimisation of the WA, the weights of the best performance are: $\mathbf{W} = [0.48\ 0.34\ 0.96\ 0.03\ -0.82]$. The cost results are shown in Table 1.

It can be see that the NARNET method performs worse than the WA when the outliers are included in the data, which is consistent with our previous work presented in ref. [30]. However, for the scenario of triple price without outliers and weekends, the NARNET is below 1% difference compared to the perfect information case over 2 years, which showcases the forecasting capacity of this method in terms of total cost.

The features of the proposed system compares to similar works in the literature are shown in Table 2.

## 6 | CONCLUSION AND FUTURE WORK

In this paper, a hierarchical distributed control framework is presented for distributed control in microgrids. The control framework has two layers (primary and secondary) for purposes of optimal cost operation of a single microgrid but can also be extended to any number of microgrids. The stability and resiliency of the proposed hierarchical control framework is then carefully validated with the use of Lyapunov stability and graph theory analysis. At the same time, it is verified that the control system designed is also capable of achieving supply cost optimisation with the use of auto-regression models for price forecast. Two forecast methods were compared, MCMC and NARNET, where the latter showed better economic performance. Each method is compared against the ideal case in terms of total cost when applied to a distributed MAS-based secondary control.

As expected from our previous precision analysis in ref. [2], the MCMC method is better suited for data with outliers in terms of cost, while the NARNET approach is better at minimising cost when the training data set does not have such outliers.
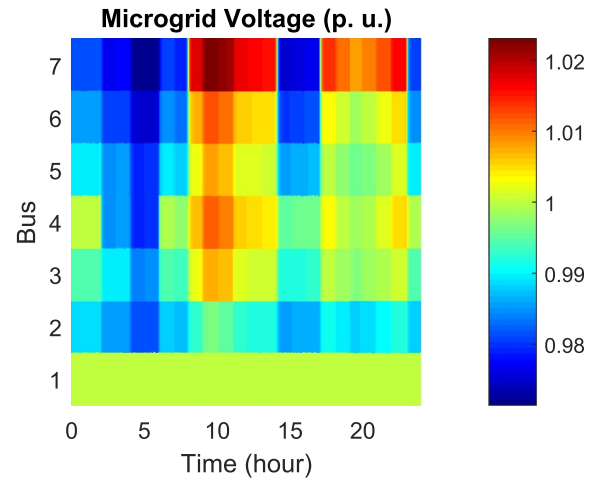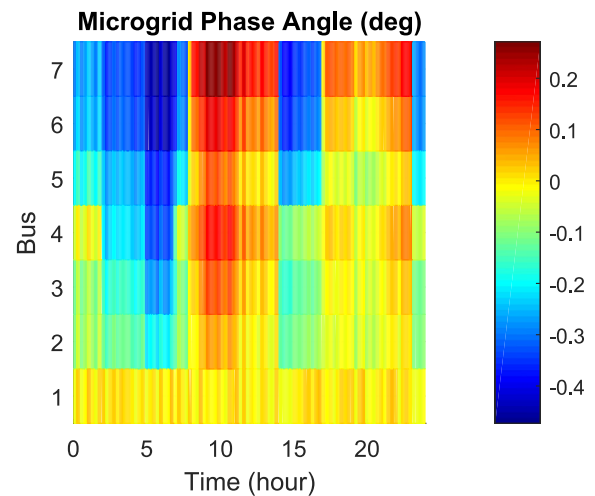
The conditions for stability for the primary level control is analysed with the direct Lyapunov method considering both the resistive and reactive components in a short-line model.

The system developed in this work has shown that it may continue stable operation within allowed margins even in events of DER disconnection and instantaneous changes in the load, which is equivalent to connection and disconnection of loads over time.

The control system has shown that is capable to operate at real time and can transition between loads, within the UK standard of voltage variations for the mains grid with varying loads.

The fact that the control system presented is capable to operate with the implementation of micro-controllers shows that the control system is not computationally expensive even with the UDP fault-tolerance mechanism. However, the ping between the nodes can be adjusted to accommodate the computational resources available.

**TABLE 1** Total Cost comparison (GBP)

| Price | Scenario | Perfect information | NARNET | WA |
|-------|----------|---------------------|--------|-----|
| Double | No weekends, no outliers | 17,285.19 | 18,358.56 | 19,317.81 |
| | No weekends no outliers all data | 17,250.52 | 19,103.90 | 19,384.47 |
| | | 24,243.42 | 26,046.88 | 27,929.09 |
| | | 24,259.32 | 27,248.01 | 27,983.01 |
| Triple | No weekends, no outliers | −12,470.42 | −11,733.26 | −11,631.11 |
| | No weekends no outliers all data | −13,908.33 | −12,348.67 | −12,913.53 |
| | | −17,185.72 | −15,063.10 | −15,868.16 |
| | | −18,513.67 | −16,140.25 | −16,712.16 |

Abbreviation: NARNET, Non-linear auto-regression Network.

**TABLE 2** Operation and Control System features comparison

| Features | [4, 5] | [2, 13–15] | Proposed system |
|----------|--------|-----------|-----------------|
| Control paradigm | Centralised | Centralised or distributed | Distributed |
| Large signal transient stability demonstrated | ✓ | ✗ | ✓ |
| Steady-state stability demonstrated | ✗ | ✓ | ✓ |
| Resilient control design | ✗ | ✓ | ✓ |
| Real-time operation demonstrated | ✗ | ✗ | ✓ |
| Optimal cost ability | ✗ | ✓ | ✓ |

The combined features demonstrated in this work validates the system design compared to similar works, as the proposed system is stable, resilient, cost efficient and compatible with real-time operation, contributing to solve the simultaneous integration of all of these features.

Our future work includes improvement on the design method to facilitate the implementation of different resources, such as renewable generation. Additionally, consideration of more complex circuits for the stable and resilient operation, such as microgrid clusters. Lastly, further development of forecast methods suitable for real-time distributed control to optimise the use of distributed generation and the interaction of the microgrid with other microgrids and the main grid.

## AUTHOR CONTRIBUTIONS
**Marcos Eduardo Cruz Victorio**: Writing – original draft preparation. **Behzad Kazemtabrizi**: writing – review and editing; supervision. **Mahmoud Shahbazi**: writing – review and editing; supervision. All authors have read and agreed to the published version of the manuscript.

## CONFLICT OF INTEREST
The authors declare no conflict of interest.

## PERMISSION TO REPRODUCE MATERIALS
None.

## DATA AVAILABILITY STATEMENT
The data that support the findings of this study are available from Nord pool. Restrictions apply to the availability of these data.

## ORCID
*Marcos Eduardo Cruz Victorio* https://orcid.org/0000-0003-2604-176X
*Mahmoud Shahbazi* https://orcid.org/0000-0002-6057-3228

## REFERENCES
1. Olivares, D.E., et al.: Trends in microgrid control. IEEE Trans. Smart Grid. 5(4), 1905–1919 (2014). https://doi.org/10.1109/tsg.2013.2295514
2. Han, Y., et al.: Mas-based distributed coordinated control and optimization in microgrid and microgrid clusters: a comprehensive overview. IEEE Trans. Power Electron. 33(8), 6488–6508 (2018). https://doi.org/10.1109/TPEL.2017.2761438
3. Morstyn, T., Hredzak, B., Agelidis, V.G.: Control strategies for microgrids with distributed energy storage systems: an overview. IEEE Trans. Smart Grid. 9(4), 3652–3666 (2018). https://doi.org/10.1109/TSG.2016.2637958
4. Huang, T., Gao, S., Xie, L.: A neural lyapunov approach to transient stability assessment of power electronics-interfaced networked microgrids. IEEE Trans. Smart Grid. 13(1), 106–118 (2022). https://doi.org/10.1109/TSG.2021.3117889
5. Kabalan, M., Singh, P., Niebur, D.: Large signal lyapunov-based stability studies in microgrids: a review. IEEE Trans. Smart Grid. 8(5), 2287–2295 (2017). https://doi.org/10.1109/TSG.2016.2521652
6. Kabalan, M., Singh, P., Niebur, D.: A design and optimization tool for inverter-based microgrids using large-signal nonlinear analysis. IEEE

Trans. Smart Grid. 10(4), 4566–4576 (2019). https://doi.org/10.1109/TSG.2018.2864208

7. Mehrasa, M., et al.: Dynamic model, control and stability analysis of mmc in HVDC transmission systems. IEEE Trans. Power Deliv. 32(3), 1471–1482 (2017). https://doi.org/10.1109/TPWRD.2016.2604295

8. Fan, Z., et al.: Operation loss minimization targeted distributed optimal control of DC microgrids. IEEE Syst. J. 15(4), 5186–5196 (2021). https://doi.org/10.1109/JSYST.2020.3035059

9. Makrygiorgou, D.I., Alexandridis, A.T.: Distributed stabilizing modular control for stand-alone microgrids. Appl. Energy. (210), 925–935 (2018). https://doi.org/10.1016/j.apenergy.2017.07.085

10. Li, T., et al.: Research on ac microgrid with current-limiting ability using power-state equation and improved lyapunov-function method. IEEE J. Emerg. Sel. Top. Power Electron. 9(6), 7306–7319 (2021). https://doi.org/10.1109/JESTPE.2020.3013230

11. Samuel, O., et al.: Towards real-time energy management of multi-microgrid using a deep convolution neural network and cooperative game approach. IEEE Access. 8, 161377–161395 (2020). https://doi.org/10.1109/ACCESS.2020.3021613

12. Liu, Y., et al.: Distributed real-time optimal power flow control in smart grid. IEEE Trans. Power Syst. 32(5), 3403–3414 (2017). https://doi.org/10.1109/TPWRS.2016.2635683

13. Li, Q., et al.: Networked and distributed control method with optimal power dispatch for islanded microgrids. IEEE Trans. Ind. Electron. 64(1), 493–504 (2017). https://doi.org/10.1109/TIE.2016.2598799

14. Zhao, T., Ding, Z.: Distributed agent consensus-based optimal resource management for microgrids. IEEE Trans. Sustain. Energy. 9(1), 443–452 (2018). https://doi.org/10.1109/TSTE.2017.2740833

15. He, Y., Wang, W., Wu, X.: Multi-agent based fully distributed economic dispatch in microgrid using exact diffusion strategy. IEEE Access. 8, 7020–7031 (2020). https://doi.org/10.1109/ACCESS.2019.2959600

16. Cvetković, D., Rowlinson, P., Simić, S.: Graph operations and modifications. In: An Introduction to the Theory of Graph Spectra, Ser. London Mathematical Society Student Texts, pp. 24–51. Cambridge University Press (2009). https://doi.org/10.1017/CBO9780511801518.003

17. Cvetkovic, D., Rowlinson, P., and Simi, S.: Laplacians. In: An Introduction to the Theory of Graph Spectra, Ser. London Mathematical Society Student Texts, pp. 184–227. Cambridge University Press (2009). https://doi.org/10.1017/CBO9780511801518.008

18. Ding, L., Han, Q., Zhang, X.: Distributed secondary control for active power sharing and frequency regulation in islanded microgrids using an event-triggered communication mechanism. IEEE Trans. Ind. Inf. 15(7), 3910–3922 (2019). https://doi.org/10.1109/TII.2018.2884494

19. Cruz Victorio, M.E., Kazemtabrizi, B., Shahbazi, M.: Distributed real-time power management in microgrids using multi-agent control with provisions for fault-tolerance. In: 2020 IEEE 29th International Symposium on Industrial Electronics, pp. 108–113. ISIE (2020)

20. Kanellos, F.D.: Real-time control based on multi-agent systems for the operation of large ports as prosumer microgrids. IEEE Access 5, 9439–9452 (2017). https://doi.org/10.1109/ACCESS.2017.2706091

21. Wu, L., Shahidehpour, M.: A hybrid model for day-ahead price forecasting. IEEE Trans. Power Syst. 25(3), 1519–1530 (2010). https://doi.org/10.1109/TPWRS.2009.2039948. ISSN: 1558-0679

22. Harlim, J.: Data-Driven Computational Methods: Parameter and Operator Estimations. Cambridge University Press (2018)

23. Kim, I.: Markov chain Monte Carlo and acceptance–rejection algorithms for synthesising short-term variations in the generation output of the photovoltaic system. IET Renew. Power Gener. 11(6), 878–888 (2017). https://doi.org/10.1049/ietrpg.2016.0976. ISSN: 1752-1424

24. Yang, X., et al.: A reliability assessment approach for electric power systems considering wind power uncertainty. IEEE Access. 8, 12467–12478 (2020). https://doi.org/10.1109/ACCESS.2020.2966275. ISSN: 2169-3536

25. Zhang, G., et al.: Forecasting time series albedo using narnet based on eemd decomposition. IEEE Trans. Geosci. Rem. Sens. 58(5), 3544–3557 (2020). https://doi.org/10.1109/tgrs.2019.2958048

26. Wan, C., et al.: A hybrid approach for probabilistic forecasting of electricity price. IEEE Trans. Smart Grid. 5(1), 463–470 (2014). https://doi.org/10.1109/TSG.2013.2274465. ISSN: 1949-3061

27. Mosbah, H., El-hawary, M.: Hourly electricity price forecasting for the next month using multilayer neural network. Can. J. Electr. Comput. Eng. 39(4), 283–291 (2016). https://doi.org/10.1109/cjece.2016.2586939

28. Du, Y., Li, F.: Intelligent multi-microgrid energy management based on deep neural network and model-free reinforcement learning. IEEE Trans. Smart Grid. 11(2), 1066–1076 (2020). https://doi.org/10.1109/TSG.2019.2930299

29. Cruz Victorio, M.E., Kazemtabrizi, B., Shahbazi, M.: Real-time cost optimisation for power management in microgrids using multi-agent control. In: 2019 9th International Conference on Power and Energy Systems, pp. 1–6. ICPES (2019)

30. Cruz Victorio, M.E., Kazemtabrizi, B., Shahbazi, M.: Price forecast methodologies comparison for microgrid control with multi-agent systems. In: 2021 IEEE Madrid PowerTech, pp. 1–6 (2021)

31. Llorente, F., Martino, L., Delgado, D.: Parallel metropolis–hastings coupler. IEEE Signal Process. Lett. 26(6), 953–957 (2019). https://doi.org/10.1109/LSP.2019.2913470. ISSN: 1558-2361

32. Priddy, K.L., Keller, P.E.: Artificial Neural Networks: An Introduction, pp. 1–12. SPIE (2005). https://doi.org/10.1117/3.633187

33. Terrell, W.J.: Chapter nine cascade systems. In: Stability and Stabilization, pp. 189–211. Princeton University Press (2009). https://www.degruyter.com/princetonup/view/book/9781400833351/10.1515/9%20781400833351-011.xml

34. Haddad, W.M., Chellaboina, V.: Chapter three stability theory for nonlinear dynamical systems. In: Nonlinear Dynamical Systems and Control, pp. 135–206. Princeton University Press (2008). https://www.degruyter.com/princetonup/view/book/9781400841042/10.1515/9%20781400841042-005.xml

35. Terrell, W.J.: Chapter eight stability theory. In: Stability and Stabilization, pp. 161–188. Princeton University Press (2009). [Online]. https://www.degruyter.com/princetonup/view/book/9781400833351/10.1515/9%20781400833351-010.xml

36. Çetinkaya, E.K., et al.: Topology connectivity analysis of internet infrastructure using graph spectra. In: 2012 IV International Congress on Ultra Modern Telecommunications and Control Systems, pp. 752–758 (2012). https://doi.org/10.1109/ICUMT.2012.6459764